




Cite this: *RSC Adv.*, 2023, 13, 5933

# Study on the surface wetting mechanism of bituminous coal based on the microscopic molecular structure

Yun Zhao,<sup>a</sup> Hongmei Li,<sup>b</sup>  <sup>\*bc</sup> Jinming Lei,<sup>b</sup> Jing Xie,<sup>c</sup> Luming Li,<sup>b</sup> Ya Gan,<sup>b</sup> Jie Deng,<sup>b</sup>  <sup>\*b</sup> Rui Qi<sup>b</sup> and Yongliang Liu<sup>a</sup>

The chemical wet dust removal method is one of the hot methods for coal dust control, and the key to its success lies in whether the surface of coal dust can be well wetted or not. Nowadays, the wetting mechanism of the coal dust surface is understudied, limiting the further application of chemical wet dust removal. Thus, the exploration of the wetting mechanism based on the microscopic molecular structure characteristics of the coal surface provides a new solution to improve the wet dust removal efficiency. Herein, the bituminous coal collected from 3 groups of coal seams in the Pingdingshan mining area was used as the object of study to reveal the microscopic wetting mechanism. Proximate analysis, nuclear magnetic resonance carbon spectroscopy (<sup>13</sup>C NMR) and X-ray photoelectron spectroscopy (XPS) can well distinguish the microstructural information of the coal surface, enabling building the molecular structure models of three groups of coal. Joint contact angle experiments were conducted to explore the influencing factors between the molecular structure of coal dust and its wettability. Molecular simulation techniques, combined with indoor experiments, were used to explore the essential causes of the differences in the wetting mechanisms of bituminous coal dust. The results showed that the composition and structure of carbon and oxygen elements on the coal surface has a significant effect on the wettability of coal dust. The higher the relative content of aromatic carbon and oxygen elements, the better the wettability of the coal surface. An opposite trend occurred for the aliphatic carbon. The difference in wettability of coal surfaces mainly stems from the ability of hydrophilic functional groups on coal surfaces to form hydrogen bonds with water molecules. The aromatic hydrocarbon structure has a much greater ability to adsorb water molecules than the aliphatic hydrocarbon structure. The research results can provide scientific guidance for the design of efficient and environmentally friendly dust suppressants to realize clean coal production in mines.

Received 11th December 2022  
Accepted 1st February 2023

DOI: 10.1039/d2ra07908a

rsc.li/rsc-advances

## Introduction

From the perspective of resource endowment characteristics, coal resources have been always dominating the primary energy consumption in China to meet the social and economic development.<sup>1</sup> In recent years, with the increase of coal mining, high production and efficient mechanized underground operations often lead to excessive dust concentration at the working face.<sup>2</sup> This difficult-to-prevent/control dust will induce a cascade of consequences such as frequent coal dust disasters, high difficulty in mining resources, deterioration of the operating environment, dust explosions and other high risks. In addition, prolonged exposure to excessive coal dust underlies

pneumoconiosis in miners.<sup>3</sup> Therefore, efficient and clean coal dust control is crucial to the mining safety and workers' occupational health.<sup>4</sup> Especially in the context of "double carbon revolution", coal dust pollution control is related to the green development of the coal industry, ecological environment protection, and national health care.

Coal surface wettability is the key to effective dust reduction during coal mining.<sup>5</sup> The existing dust removal technologies mainly include different dust source control and removal technologies such as local fogging closure, air curtain isolation, wind and fog double curtain synergistic efficiency, coal seam water injection, and mine wet spray operations system.<sup>6</sup> All of the above technologies are developed on the basis of the wettability of coal surface. More than two-thirds of coal seams in China are difficult to wet.<sup>7</sup> Therefore, it is vital to study the coal surface wettability to improve the effectiveness of coal dust control. Cheng *et al.*<sup>8</sup> concluded that primary minerals represented by quartz among the inorganic minerals contained in coal are the most important factors to improve the hydrophilicity of the coal

<sup>a</sup>School of Mechanical Engineering, Chengdu University, Chengdu, 610106, China

<sup>b</sup>College of Food and Bioengineering, Chengdu University, Chengdu, 610106, China.  
E-mail: lihongmei@cdu.edu.cn; dengjie@cdu.edu.cn

<sup>c</sup>State Key Lab of Hydraulics and Mountain River Engineering, College of Water Resource & Hydropower, Sichuan University, Chengdu, Sichuan 610065, China



surface. Wang *et al.*<sup>9</sup> analyzed the coal quality characteristics of typical medium and low rank coals and showed that the intensity of absorption peaks of hydrophilic functional groups on the coal surface gradually decreased as the degree of coal metamorphism increased, and the hydrophilic functional groups were positively correlated with the wettability of the coal surface. Xie *et al.*<sup>10</sup> analyzed the fitted relationships between the changes in ash content, mineral element composition, and functional groups and wettability of coal after acid treatment, and found that acid treatment reduced the ash content and coal surface wettability. The changes both in Si and Al elements in inorganic mineral elements and in hydroxyl peak area in oxygen-containing functional groups were consistent with the wettability evolution.

For a long time, research has focused on the influence of experimental aspects such as coal composition and surface chemical structure on wettability. With the continuous development of computer technology, molecular simulation techniques are increasingly applied to study the mechanisms of the wettability of coal surfaces. Yuan *et al.*<sup>11</sup> investigated the wetting and adsorption of two surfactants on low-rank coal by combining macroscopic experiments and molecular dynamics simulations. The results showed that cocoamidopropyl betaine (CAB) formed more hydrogen bonds with coal than coconut diethanol amide (CDEA), thus imparting superior wetting and adsorption properties to low-rank coal. Li *et al.*<sup>12</sup> investigated the regulation mechanism of dodecyl ethoxyl ethers ( $C_{12}EO_n$ ) on the wettability of low-rank coal using density functional theory (DFT) calculations and molecular dynamics (MD) simulations. The results unveiled that the hydrophilicity sequence for the models was determined as benzoic acid > phenol > ether > methylbenzene, and the regulation effect of dodecyl ethoxyl ethers on the wettability of low-rank coal was governed by the ethylene oxide (EO) number.

Many scholars have paid attention to studying the wettability of coal surfaces using a combination of laboratory experiments and computational simulations. In the study of the coal dust wetting mechanism, a large number of research studies have provided valuable experience for the application of molecular simulations. Meng *et al.*<sup>13</sup> used the Materials Studio 8.0 molecular simulation software to deeply analyze the mechanism of the wetting system of three kinds of coal samples with different metamorphic degrees. From the microscopic perspective of adsorption spacing, adsorption sites and “reverse adsorption” phenomenon, it was revealed that the higher the degree of coal metamorphism, the worse the wettability of coal. Feng *et al.*<sup>14</sup> characterized the coal samples from Hongshiwan (HSW) mining area by using solid state  $^{13}C$  nuclear magnetic resonance ( $^{13}C$  NMR), X-ray photoelectron spectroscopy (XPS) and Fourier transform infrared spectroscopy (FT-IR). Then the key information about elements, valence, and chemical bonding for coal molecular structural construction is obtained. Zhang *et al.*<sup>15</sup> constructed the large-scale molecular structure of Fenghuangshan anthracite by combining XRD, XPS,  $^{13}C$  NMR and high-resolution transmission electron microscopy (HRTEM). The structure captures the crystalline characteristics, aromaticity,

organization, molecule curvature, heteroatom functionality, and much of the micropore size distribution, which is expected to provide practical value for exploring coalification, heat treatment and microstructures. However, the difference of wettability of bituminous coal through independently constructed coal molecules still lacks specificity.

In this paper, three groups of coals in the Pingdingshan coal mining area were selected to reveal the relationship between the coal surface composition structure and wetting structure. In order to systematically investigate the main factors affecting the wettability of coal surfaces, microscopic molecular structure analysis was performed on coal samples. Analytical tests such as proximate analysis, nuclear magnetic resonance carbon spectroscopy ( $^{13}C$  NMR) and X-ray photoelectron spectroscopy (XPS) were used to examine the chemical composition of coal samples, organic molecular structure carbon skeleton and the influence of elemental composition on the surface wettability of coal. A well-constructed wetting and sorption model for bituminous coal can well reveal the preliminary wetting mechanism of the microscopic molecular structure characteristics of coal surfaces, which provides technical guidance and research ideas for scientific and efficient chemical dust removal in China.

## Materials and methods

### Sample preparation

The coal samples were collected from the Ding 5-22190 (A), Wu 8-31220 (B) and Ji 15-31020 (C) coal seams in the no. 12 mining area of Pingdingshan, Henan Province. After air-drying, the coal samples were crushed with an XQM-0.4 planetary ball mill and passed through 200 mesh sieves to produce the coal samples with particle sizes less than 0.075 mm. The test coal samples were fully dried at 60 °C. The three groups of coal samples did not settle in pure water for 24 hours and had poor wetting performance.<sup>16</sup>

Proximate analysis is the most basic method to determine the composition of coal. An XKGF-8000 Automatic Industrial Analyzer of the State Key Laboratory of Coking Coal Resources Development and Comprehensive Utilization was used for the determination. Proximate analysis was conducted according to Chinese National Testing Standard (GB/T 212-2008), and the experimental results are shown in Table 1.

### Contact angle test

The contact angle ( $\theta$ ) can vividly characterize the wettability of coal surfaces, and is the angle formed at the junction of gas-

Table 1 Proximate analysis of coal samples

Coal sample	Proximate analysis (wt%)			
	$M_{ad}$	$A_{ad}$	$V_{daf}$	$FC_{ad}$
A	1.07	32.34	35.59	43.03
B	1.35	45.90	36.23	33.87
C	1.81	9.37	24.47	67.22



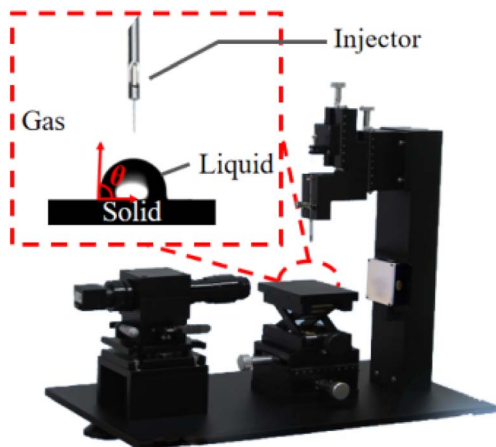


Fig. 1 Schematic diagram of contact angle measurement.

Table 2 Contact angle test results of coal samples

Coal sample	Contact angle $\theta$ (°)		
	Distilled water	Formamide	Diiodomethane
A	83.5	46.0	34.3
B	66.4	32.5	33.5
C	93.3	61.0	47.6

liquid-solid phases when a liquid droplet wets a solid surface.<sup>17</sup> The smaller the  $\theta$ , the better the coal surface wettability. In order to characterize the wetting variability of pure water on the three groups of coal, the JC2000D1 (Shanghai Powereach) contact angle measuring instrument was used to test their wettability. The measurement is shown in Fig. 1. 300 mg of the test coal sample was pressed in the mold of HY-12 tablet at 30 MPa for 1 min to obtain smooth discs with a diameter of about 10 mm and a thickness of about 2 mm. Using a micro syringe, appropriate amounts of deionized water, formamide and diiodomethane were aspirated to form a 4  $\mu$ l droplet above the flake coal sample for titration. The contact angle between the droplet and the coal piece was repeatedly measured three times to obtain an average contact angle value. The contact angle data of the coal samples are shown in Table 2.

## The NMR experiment

The basic skeleton of coal is carbon, and nuclear magnetic resonance (NMR), one of the modern instrumental analysis techniques, can directly study the microscopic chemical structure of coal without damage. A solid-state NMR spectrometer (AVANCE III 500 MHz) at the Analysis and Testing Center of Sichuan University was used to analyze the structural composition of the coal samples. The resonance frequency of the detection nucleus was 100.38 MHz, and a 4 mm solid-state H-Y-X triple resonance MAS probe was used with a magic angle speed of 5 kHz, a cycle delay time of 2 s, and a scan number of 10 240–20 480 times. To obtain the ideal spectra, the determination was performed using cross-polarization (CP) and suppression of sidebands (TOSS) techniques. In order to avoid the influence of minerals during the test, hydrochloric acid washing followed by a hydrofluoric acid wash was used for mineral removal. The chemical shifts of the peaks in the  $^{13}\text{C}$  NMR spectra can characterize the carbon skeleton functional groups to further reveal the coal's chemical structure. The fitted curves of the peaks of the coal samples are shown in Fig. 2.

## The XPS experiment

The XPS experimental analysis of the surface properties of coal dust was carried out using a PHI 5000 (Ulvac-PHI, Inc., Kanagawa, Japan) X-ray photoelectron spectrometer. The detailed experimental conditions were as follows: an excitation source of monochromatic Al K $\alpha$  X-rays. The energy resolution was  $\Delta E \leq 0.5$  eV. The obtained binding energy was calibrated with C 1s (284.6 eV) as the internal reference standard. Data evaluation was carried out with the Gaussian/Lorentzian function. A Shirley background was used, and elemental composition was characterized *via* the quantitative peak method. The XPS spectra of the samples and the peak diagrams from the spectra are shown in Fig. 3.

## Experimental results and analysis

### Proximate analysis of coal samples and the effect on wettability

As seen in Table 1,  $M_{\text{ad}}$  is the air dry basis moisture in coal samples,  $A_{\text{ad}}$  is the air dry basis ash content,  $V_{\text{daf}}$  is the dry ash-free

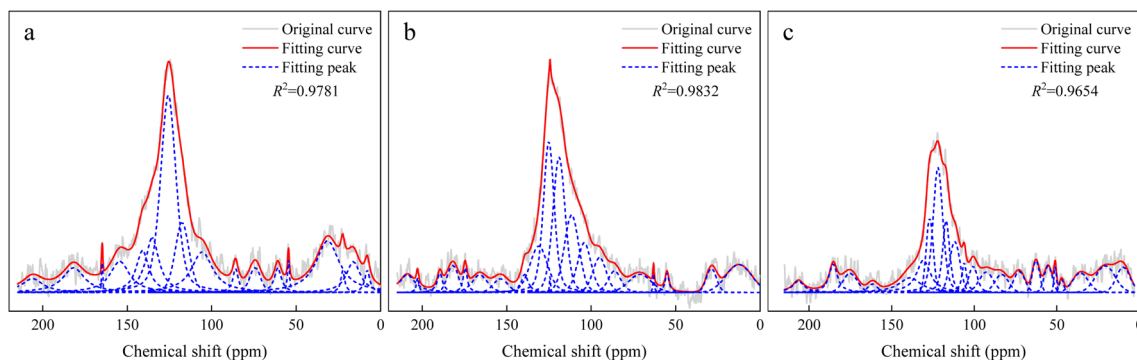


Fig. 2 Curve-fitting  $^{13}\text{C}$  NMR spectra of Coals (a) A, (b) B, and (c) C.

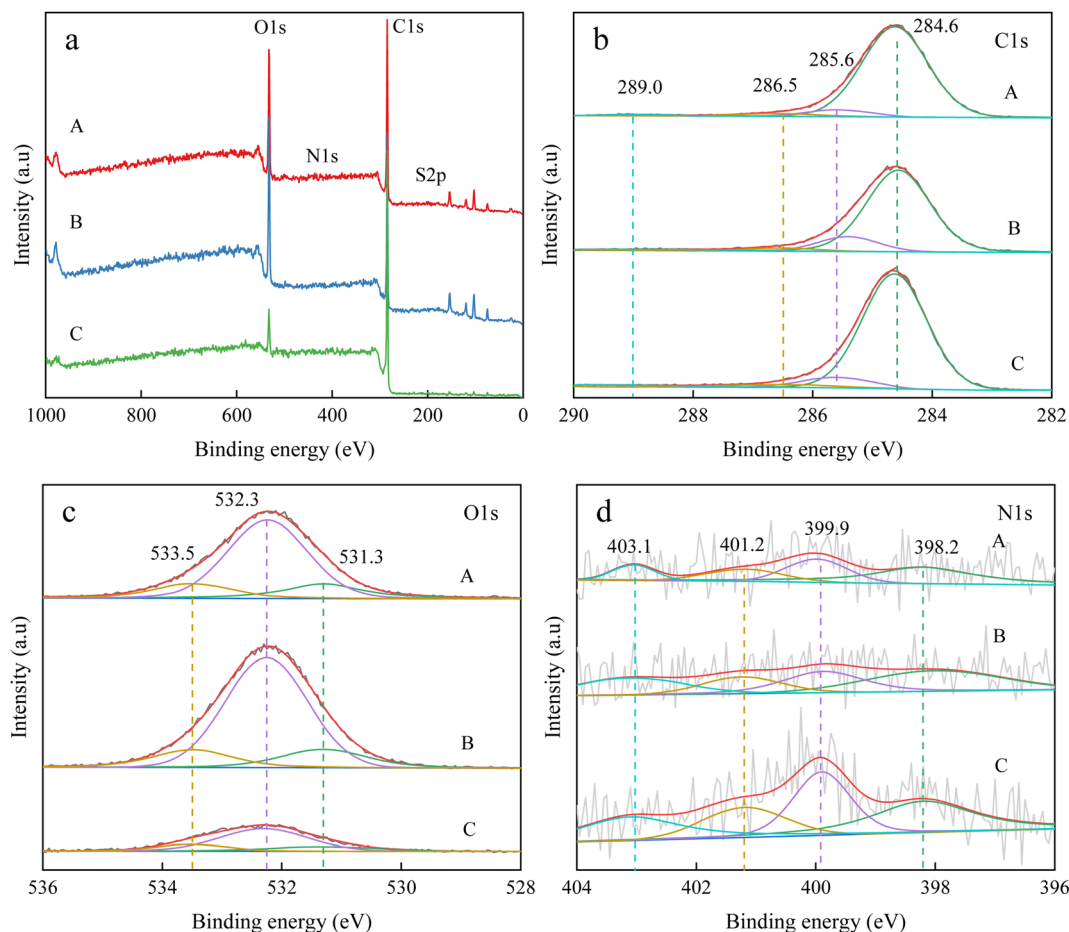


Fig. 3 XPS spectra of coal samples: (a) wide spectra. (b) C 1s. (c) O 1s. (d) N 1s.

basis volatile matter, and  $FC_{ad}$  is the air dry basis fixed carbon. According to China Coal Classification Standard (GB/T 5751-2009), a dry ash-free basis volatile fraction ( $V_{daf}$ ) content between 10.0 and 37.0% is bituminous coal. The differences in volatile matter, fixed carbon, moisture, and ash in the three groups of bituminous coals are large. The moisture content is comparatively low, fixed carbon content increases in the order of  $C > A > B$ , and the ranking of ash content is  $B > A > C$ . Among the three groups of coal samples, the contact angle between the group B coal sample and water was the smallest ( $66.4^\circ$ ), indicating its best surface wettability. The contact angle of the coal sample of group A was  $83.5^\circ$ , and the surface wettability of coal of group A was the second. The contact angle of the coal sample of group C is the largest,  $93.3^\circ$ , and the wettability is the worst. The order of the wettability of the coal of 3 groups in pure water is  $B > A > C$ .

The surface wettability of the three groups of coal samples is positively correlated with the ash content and negatively correlated with the fixed carbon content. This stems from both the enhanced wettability of bituminous coals due to the primary minerals in the ash and from the fact that the organic molecular structure represented by the fixed carbon is the relative hydrophobic composition of the surface.<sup>8,18</sup>

The surface wettability of coal samples was almost uncorrelated with moisture content, which may be due to the similar

coal-forming periods and regional deposition conditions of the same bituminous coal, resulting in a similar surface pore structure and small difference in adsorbed free water content of the coal surface. Therefore, the moisture content has a small effect on the wettability of coal in the Pingdingshan coal mining area.<sup>19,20</sup> The surface wettability of coal was also positively correlated with volatile content, but the correlation was weaker compared with its fixed carbon and ash content. It can be seen that the fixed carbon and ash content are the main factors affecting the wettability of bituminous coal.

Among the three groups of coal samples, the B group has the smallest fixed carbon content and the largest ash content, and the best wettability. The wettability of group C was the worst due to the largest fixed carbon content and the lowest ash content.

#### Analysis of the carbon skeleton of coal samples and the effect on wettability

It is obvious from the fitted curves of the peaks of the coal samples that the peaks of the three groups of bituminous coals have similar peak shapes. The  $^{13}C$  NMR spectra of coal can be categorized into four types of C atoms in the range of 0–220 ppm, as shown in Table 3, with peaks at 0–50 ppm attributed to aliphatic carbon peaks, 50–90 ppm to ether-oxygen





**Table 3** Structural attribution of chemical shifts in the  $^{13}\text{C}$ -NMR spectra of coal

Chemical shift range (ppm)	Carbon type
0–16	R-CH <sub>3</sub>
16–20	Ar-CH <sub>3</sub>
20–23	CH <sub>2</sub> -CH <sub>3</sub>
23–35	CH <sub>2</sub>
36–50	C, CH
50–60	O-CH <sub>3</sub> , O-CH <sub>2</sub>
60–75	O-CH
75–90	R-O-R
90–129	Ar-H
129–137	Bridgehead
137–150	Ar-C
150–170	Ar-O
170–190	-COOH
190–220	>C=O

carbon peaks, 90–165 ppm to aromatic carbon peaks, and 165–220 ppm to carboxyl and carbonyl carbon peaks.<sup>21,22</sup> The intensity of the aromatic carbon peak is the strongest among the three groups of coal samples, indicating that aromatic carbon is the main component of the molecule in bituminous coals from the Pingdingshan coal mining area.

The carbon structure parameters were obtained from the chemical shifts of the fitted characteristic peaks and their areas as shown in Table 4. From Table 4, it can be seen that the aromatic carbon content of all three groups of bituminous coals is much larger than that of aliphatic carbon, and the  $\text{sp}^2$  hybridized carbon ( $f_a$ ) is 74.55% (A), 82.90% (B) and 72.57% (C). This result is similar to that of the primary coal from Pingdingshan mine tested by Guo *et al.*<sup>23</sup> in the range of 72.72–81.70%.

The  $\text{sp}^2$  hybrid carbon is mainly composed of two parts: aromatic carbon ( $f'_a$ ) and carbonyl carbon ( $f_a^C$ ), and the aromatic carbon content is larger than the carbonyl carbon content. The aromatic carbon ( $f'_a$ ) consists of protonated aromatic carbon ( $f_a^H$ ) and nonprotonated aromatic carbon ( $f_a^N$ ), and the nonprotonated aromatic carbon ( $f_a^N$ ) comprises three parts: phenolic hydroxyl or ether-oxygen carbon ( $f_a^P$ ), alkyl-substituted aromatic carbon ( $f_a^S$ ) and bridging aromatic carbon ( $f_a^B$ ).<sup>24</sup> The phenolic hydroxyl or ether-oxygen carbon ( $f_a^P$ ) represents the distribution of oxygen-containing functional groups in coal, and the carbonyl carbon ( $f_a^C$ ) and ether-oxygen carbon ( $f_a^P$ ) are less in the three groups of coal

samples, suggestive of the smaller level of the oxo-functionalities in coals.

Aliphatic carbon ( $\text{sp}^3$  hybridized carbon,  $f_{al}$ ) exists in the form of aliphatic side chains to link the aromatic hydrocarbon structural units, and includes methyl ( $f_{al}^*$ ), quaternary carbon and methylene ( $f_{al}^H$ ), and oxygen-linked aliphatic carbon ( $f_{al}^O$ ). The characteristic parameters of the aliphatic hydrocarbon structures ( $f_{al}^*$ ) of the B and C coals are greater than those of methylene ( $f_{al}^H$ ), uncovering their higher degree of branched-chains. Meanwhile, in addition to the trace methylene and methine, their aliphatic carbon atoms mainly adopt the methyl, in poignant contrast with the A group coals. These data clarify the coal's carbon skeleton of the dominating aromatic carbon (>60%) and the secondary aliphatic one (<30%), with both aromatic carbon ( $f'_a$ ) ( $B > A > C$ ) and aliphatic carbon level ( $B < A < C$ ) distinct across samples.

Reportedly, the aromatic and aliphatic hydrocarbons of the coal's carbon skeleton are hydrophobic.<sup>25</sup> The contact angle of coal samples gradually decreases and the surface wettability increases as the aromatic carbon content of coal samples increases, indicating that aromatic hydrocarbons contribute more to the surface wettability of coal than aliphatic hydrocarbon structures. Kozbial *et al.*<sup>26</sup> found that water for conjugated molecules exhibited enhanced affinity for hydrogen atoms that can be preferentially adsorbed and directed towards the non-polar  $\text{sp}^2$  hybrid carbon structure compared to  $\text{sp}^3$  hybrid carbon. Since  $\pi$ -H bonds contribute to the stronger interaction between nonpolar  $\text{sp}^2$  hybrid carbon and water, water molecules are biased towards adsorption at coal's aromatic hydrocarbon structure. Clearly, the coal surface wettability improves on the increasing aromatic ring carbon structure when the aromatic carbon content of bituminous coal is 62–74%.

### Analysis of elemental composition of coal samples and effects on wettability

The elemental composition of coal samples and their morphology govern the wetting performance.<sup>27</sup> Firstly, the XPS spectra were detected to examine the coal's surface information.

Fig. 3(a) shows the XPS wide scan spectra of all coal samples. Only the dominating peaks of C 1s (285 eV) and O 1s (533 eV) occur, indicating the very high carbon and oxygen contents.<sup>28</sup> The intensity of the absorption peak of C 1s is significantly stronger than that of O 1s, showing the much higher carbon contents than oxygen in coals. Carbon is the main constituent

**Table 4** Structural parameters of the coals<sup>a</sup>

Coal sample	$f_a$	$f_a^C$	$f'_a$	$f_a^H$	$f_a^N$	$f_a^B$	$f_a^S$	$f_a^P$	$f_{al}$	$f_{al}^*$	$f_{al}^H$	$f_{al}^O$
A	74.55	8.33	66.22	45.17	21.05	8.21	5.93	6.91	25.45	6.55	12.51	6.40
B	82.90	9.14	73.77	58.66	15.10	8.52	1.78	4.81	17.10	6.45	2.30	8.35
C	72.57	9.77	62.80	47.87	14.93	8.17	5.74	1.02	27.43	10.55	4.58	12.31

<sup>a</sup>  $f_a$ : total  $\text{sp}^2$  carbon;  $f_a^C$ : carbonyl or carboxyl carbon  $\delta$  (chemical shift)  $>170 \times 10^{-6}$ ;  $f'_a$ : aromatic carbon;  $f_a^H$ : protonated aromatic carbon;  $f_a^N$ : nonprotonated aromatic carbon;  $f_a^B$ : aromatic bridgehead carbon;  $f_a^S$ : alkylated aromatic carbon;  $f_a^P$ : aromatic ether or phenolic hydroxyl carbon;  $f_{al}$ : total aliphatic carbon;  $f_{al}^*$ :  $-\text{CH}_3$ ;  $f_{al}^H$ :  $-\text{CH}$  or  $-\text{CH}_2$ ;  $f_{al}^O$ : bonded to oxygen.



of organic matter in coal to produce the skeleton of thick-ringed aromatic hydrocarbons.

The relative content of four detectable elements (C, O, N, and S) on the coal surface can be obtained by using the elemental sensitivity factor method, converting the peak areas to contents using elements C, O, N, and S as 100% benchmarks.<sup>29</sup> Table 5 shows the carbon content ranking of B < A < C, while the oxygen content follows the order of B > A > C. The O/C atomic ratios of A, B and C can be calculated to be 0.23, 0.31 and 0.06, respectively.

The XPS C 1s spectra of the coal samples are shown in Fig. 3(b). The peaks at 284.6, 285.6, 286.5, and 289.0 eV are attributed to C–C/C–H, C–O, C=O, and to –COOH, respectively. The C atoms of the predominant C–C/C–H peak refer to the aromatic hydrocarbon structure C in coal and its substituted alkanes. The content of aromatic hydrocarbon structure C in the coal samples of the three groups of A, B, and C reached 89.27%, 85.22% and 84.81%, respectively, indicating that the carbon in the three groups of bituminous coals is dominated by aromatic hydrocarbon structure carbon, which is consistent with the analysis of NMR results.

The peaks at 531.3, 532.3, and 533.5 eV correspondingly pertain to the carbonyl oxygen, phenolic hydroxyl and ether oxygen, and the carboxyl oxygen. Thus, the oxygen elements in the three coal samples mostly adopt the phenolic hydroxyl and ether oxygen, with the C–O relative contents being 68.86% for A, 72.17% for B, and 64.96% for C. Besides, the relative contents of hydroxyl and ether oxygen in the coal of group B were the highest.

The distribution of N atoms is shown in Fig. 3(d). The peaks at 398.2, 399.9, 401.2, and 403.1 eV typify pyridine type nitrogen, pyrrole type nitrogen, quaternary nitrogen, and nitrogen oxide nitrogen, respectively. Obviously, the nitrogen on coal surfaces principally shares the pyridine–pyrrole-type motif.

Given the indistinguishable surface sulfur signals for all samples, sulfur atoms were not considered to model the practical coal samples. The XPS analysis corroborates the same occurrence form of C, O, and N elements on all specimens, with the small N element, the high C element (90% for C group), and the medium O element (7%). Combined with the contact angle data, the higher the C element, the higher the contact angle; the smaller the O element, the greater the contact angle. This can evidence a negative or positive dependence of the coal's surface wettability upon the carbon or oxygen level, respectively. This stems from the form of assignment of carbon elements in coal, which is mainly in the form of carbon skeleton, alkyl side chains, bridge bond carbon connecting aromatic rings and carbon atoms connecting oxygen-containing functional groups at the periphery of the basic structural unit of coal. The

existence of carbon elements in coal in the form of the vast majority of hydrophobicity is stronger. Therefore, the carbon element content in coal is an important factor affecting the wettability of the coal surface: the higher carbon mitigates against its wettability.

The form of oxygen is mainly the strongly polar oxo-functionalities, such as carboxyl and phenolic hydroxyl groups. The principle of similar solubility supports their high affinity for water and thus the higher contribution to the wettability of coal. Comparatively, some less polar functional groups such as the carbonyl group, methoxy group and ether bonds can still produce hydrogen bonds with water under appropriate conditions to partway promote their hydrophilicity as a result of high electronegativity and the small radius of oxygen. Therefore, group B with relatively high oxygen content has the smallest contact angle and better wettability. In a word, the C and O content of coal's surface can act as a good proxy for inspecting the coal wettability.

### Modelling the structure of coal molecules

All above analyses signified both the compositional complexity of coals (particularly the huge disparity in the fixed carbon, aromatic carbon, aliphatic carbon, and coal surface carbon) and the strong impact of superficial oxygen upon wettability. To microscopically verify the inherency between the structure of surface organic molecules and the wetting by water molecules, the wetting mechanism on the molecular scale is further explored using an accurately constructed micromodule model based on the confirmed carbon skeleton structure composed of aromatic/aliphatic hydrocarbon structures. The ratio of aromatic bridge carbon to periplasmic carbon ( $X_{BP}$ ) reflects the average degree of condensation of aromatic rings in coal molecules and can be used to calculate *via* eqn (1) the size of aromatic clusters in coal, which is an important parameter to construct a structural model of coal molecules.

$$X_{BP} = \frac{f_a^B}{(f_a^H + f_a^P + f_a^S)} \quad (1)$$

The  $X_{BP}$  values of three groups of A, B and C were 0.14, 0.13 and 0.15, respectively, while the ones of the benzene ring, naphthalene ring and anthracene ring were 0, 0.25 and 0.4, respectively. Thus, the aromatic skeletons of the bituminous coals from Pingdingshan mine were mainly benzene and naphthalene rings with a small amount of anthracene rings. The governing pyridine- and pyrrole-type N as discovered by the XPS N 1s allows adding these two N structures into the aromatic ring to more precisely simulate the actual coal structure: 1 pyridine and 1 pyrrole to the A and B groups and 2 pyridine and 2 pyrroles to the C group.

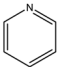
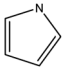
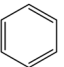
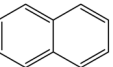
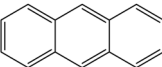
By fine-adjusting the number of benzenes, naphthalene, anthracene, and nitrogen-containing aromatic rings to make the  $X_{BP}$  value close to the experimental value, an optimal model structure with the aromatic ring carbon atoms of 147 (A), 137 (B), and 154 (C) is built as shown in Table 6.

Table 5 The component ratio of elements on the coal surface

Coal sample	C/%	O/%	N/%	S/%
A	74.77	23.50	0.99	0.74
B	69.05	28.81	1.35	0.78
C	89.96	7.14	2.38	0.52



Table 6 Types and quantities of aromatic unit structures

Coal samples	Number				
					
A	1	1	9	7	1
B	1	1	9	6	1
C	2	2	7	8	1

The parameters of  $f_{ab}$ ,  $f_{al}^*$ ,  $f_{al}^H$  and  $f_a^C$  of the coal samples were combined with XPS to derive the ratios of element and oxo-functionalities. The number was determined according to the minimum unit principle. The atom number of O or C was determined according to the minimum unit principle or the O/C atom ratio, respectively. The C atoms were finalized as 174 (A), 161 (B), and 183 (C), whilst their carbon content in the order of size accords with the fixed carbon in the proximate analysis. Besides, the number of aliphatic carbon C atoms was optimized to be 27 (A), 24 (B), and 29 (C).

Aliphatic carbons exist as methylene, methine, aliphatic side chains and cycloalkanes. The  $^{13}\text{C}$  NMR and XPS analysis can jointly quantify the methyl carbon (aliphatic methyl carbon and aromatic methyl carbon), methylene carbon/quaternary carbon and oxygen-conjugated aliphatic carbon (methoxy carbon, oxygen-conjugated methine carbon, and epoxy-conjugated aliphatic carbon): 7, 13 and 7 for group A, 9, 3 and 12 for group B, and 11, 5 and 13 for group C, respectively. For group A, both methylene and methine outnumber methyl, and the alkyl side chains are mainly long chains. As to B and C groups, methyl groups outnumber methylene ligands, and the alkyl side chains are mainly short chains.

The O/C atomic ratios of the A, B, and C coals were 0.23, 0.31, and 0.06, respectively, and the numbers of O atoms were 40, 50, and 11, respectively. The  $^{13}\text{C}$  NMR and XPS O 1s spectra inform the quantity of ether oxygen, carbonyl groups and carboxyl groups as 5, 2, and 2 for the C group coals, 28, 4, and 4 for the A group, 35, 5, and 5 for the B group coals, respectively. Nitrogen atoms mainly adopt the pyrrole-type and pyridine-type moieties. The S elements are eliminated in our molecular model due to their negligible practical contents.

The  $^{13}\text{C}$  NMR spectra of coal molecules were predicted by using MestRenova software, and the linkages of various functional groups in coal molecules were continuously adjusted to ensure that the simulated NMR spectra of the three groups of bituminous coal molecule models matched the experimental models to the maximum extent (as shown in Fig. 4) and the molecular formulae of the three groups of A, B, and C were  $\text{C}_{174}\text{H}_{116}\text{N}_2\text{O}_{40}$ ,  $\text{C}_{161}\text{H}_{94}\text{N}_2\text{O}_{50}$ , and  $\text{C}_{183}\text{H}_{140}\text{N}_4\text{O}_{11}$  after adjustment and optimization, respectively, and the final molecular structure models are shown in Fig. 5.

## Molecular simulation

### Molecular dynamics simulation

The constructed model of bituminous coal in Pingdingshan mine can profoundly depict its molecular structure characteristics to clarify the wetting phenomena of bituminous coal from the microscopic molecular mechanism. The molecular dynamics simulations were performed using the Forcite module of Materials Studio (MS) software, using the Smart method for structural optimization, with the accuracy set to medium, the COMPASS force field selected, the forcefield assigned to the charge, and the number of iteration steps of 5000. In the geometry optimization, the atom based method is used for the summation of both electrostatic and van der Waals forces, and the truncation radius is 12.5 Å.

The aggregated state model of bituminous coal was constructed from four optimized coal molecules using the Amorphous Cell (AC) module, and the energy minimization and molecular dynamics simulations were performed in the Forcite module. The molecular dynamics simulations of the aggregated state model of bituminous coal were carried out under an isobaric isothermal system (NPT) with 298 K and 0.0001 GPa pressure. The nose temperature control method and Berendsen pressure control method were chosen with 1 fs time step and 200 ps simulation time. Ewald and atom based summation were used for electrostatic interactions and van der Waals interactions, respectively.

A water layer containing 1000 water molecules is constructed using the AC module, and the bituminous coal/water system is modelled using the build layers tool. The vacuum layer of the bituminous coal/water system is set to 20 Å. The atoms of about

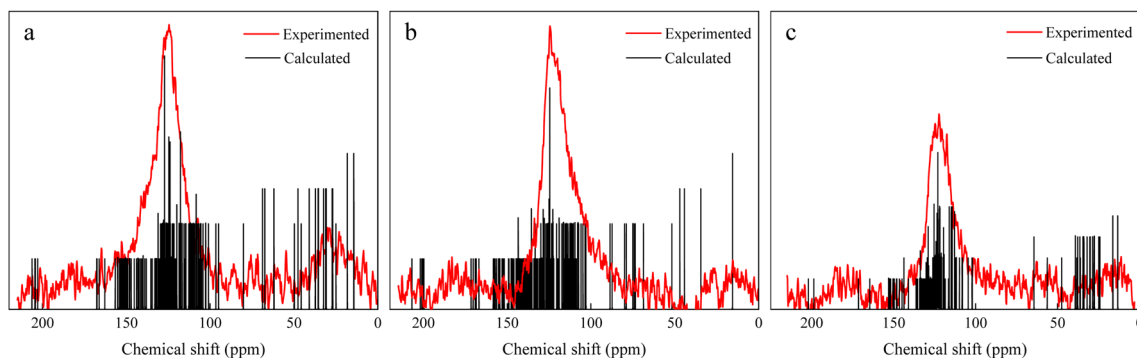


Fig. 4 Experimental and calculated spectra of  $^{13}\text{C}$  NMR: (a) A. (b) B. (c) C.



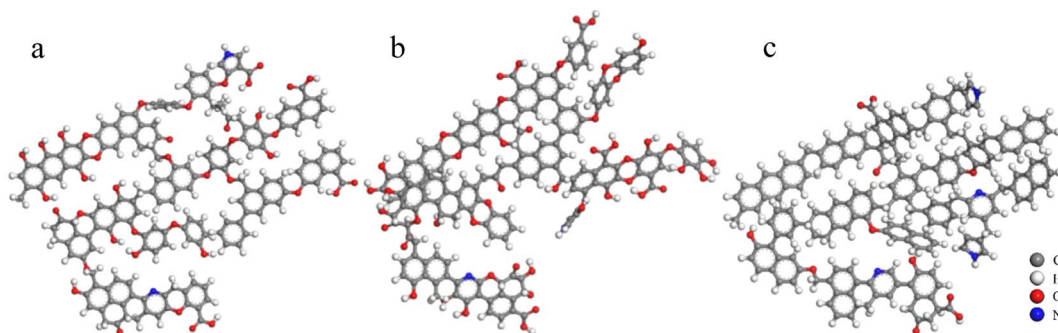


Fig. 5 Molecular structure model of coals (a) A:  $C_{174}H_{116}N_2O_{40}$ , (b) B:  $C_{161}H_{94}N_2O_{50}$ , and (c) C:  $C_{183}H_{140}N_4O_{11}$  (gray: carbon atom, white: hydrogen atom, red: oxygen atom, and blue: nitrogen atom).

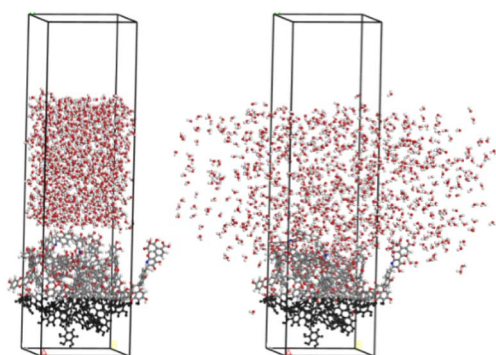


Fig. 6 Initial and equilibrium configuration of the coal–water system.

1/2 thickness at the bottom of the aggregated state model of the fixed coal are used to simulate the block structure (Fig. 6). After structural optimization of the system, simulations of 500 ps in time were performed under the regular (NVT) system synthesis, and the data of 250 ps after equilibrium were extracted for relevant analysis.

Hydrogen bonding has an important effect on the adsorption between bituminous coals and water molecules in the coal–water system, and thus the number of hydrogen bonds formed between coal and water molecules can act as a proxy of the surface wetting performance of bituminous coals. To better investigate the formation of hydrogen bonds, the hydrogen bond geometry criteria were used: the distance between intermolecular hydrogen-acceptors was less than 2.5 Å and the angle between donor-hydrogen-acceptors was greater than 135°. The number of hydrogen bonds formed between coal and water molecules was calculated by editing a Perl language script, and the number of hydrogen bonds in three systems of A, B, and C was 36, 50, and 15, respectively.

The number of hydrogen bonds shows a descending order of  $B > A > C$  and a positive nexus to surface wettability. As the oxygen-containing functional groups on the surface of coal gradually decrease, the ability to form hydrogen bonds between surface hydrophilic functional groups and water molecules is made weak, thereby yielding a decreased adsorption of water molecules on the surface of coal and the worsened surface wettability.

The hydrogen bonding interaction between coal and water molecules affects the motion state of surrounding water molecules, so the degree of influence of hydrogen bonding on water molecules can be examined by calculating the kinetic properties of water molecules. Mean Square Displacement (MSD) and self-diffusion coefficient ( $D$ ) of water molecules are used to determine the influence characteristics of water molecules produced by aggregation on the coal surface, and the calculation formula is as follows:

$$MSD = \frac{1}{N} \sum_{i=1}^N [r_i(t) - r_i(0)]^2 \quad (2)$$

$$D = \frac{1}{6N} \lim_{t \rightarrow \infty} \frac{d}{dt} \sum_{i=1}^N \{ [r_i(t) - r_i(0)]^2 \} \quad (3)$$

$$= \lim_{t \rightarrow \infty} \left( \frac{MSD}{6t} \right) = \frac{1}{6} K_{MSD}$$

where  $N$  is the number of diffusing molecules;  $r_i(t)$  and  $r_i(0)$  are the position vectors of molecules at time  $t$  and  $t = 0$ , respectively;  $K_{MSD}$  is the slope of the MSD curve, *i.e.*, the diffusion coefficient  $D$  is 1/6 of the slope of the MSD curve. The mean square displacement of water molecules at 250 ps after equilibrium of different systems is calculated as shown in Fig. 7.

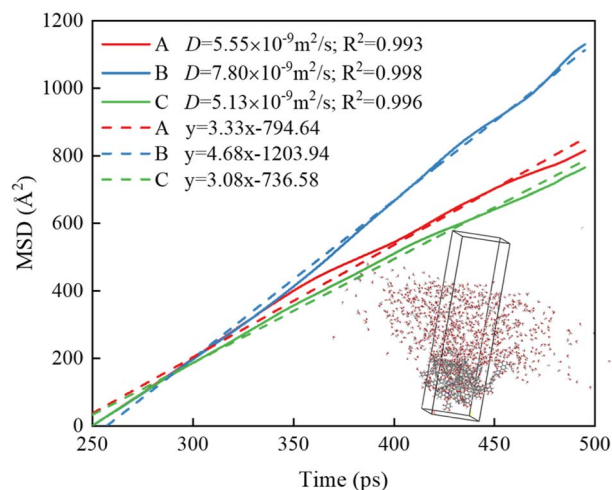


Fig. 7 MSD curves of water molecules in different systems.





The  $D$  value of water molecules in different systems ascends:  $C < A < B$ . The  $D$  value of water molecules is proportional to the number of hydrogen bonds between coal and water, and is positively correlated with the wettability, indicating that the hydrogen bonding formed between hydrophilic groups and water molecules on the coal surface promotes the migration and diffusion of water molecules toward the coal surface. The improved mobility of water molecules thus enhances the wettability of the coal surface.

The radial distribution function (RDF) method is used to further analyze the effect of coal surface oxygen on the hydrogen bonding interaction between coal and water molecules. RDF is a function that describes the relationship between the spatial distribution probability of a specific particle and the distance of a reference particle. Usually, certain particle coordinates are specified to calculate the probability of distribution of other particles in space. The RDF of particle B around particle A is expressed by the following equation:

$$G_{A-B}(r) = \left[ \frac{1}{(4\pi r^2 \rho_B)} \right] (dN_{A-B}/dr) \quad (4)$$

where  $\rho_B$  is the number density of particle B,  $r$  is the distance between particle B and particle A, and  $dN_{A-B}$  is the average number of particles B in the region  $r$  around particle A as the reference particle. The relative probability of the occurrence of hydrogen atoms of water molecules ( $H_{\text{water}}$ ) centered on oxygen atoms ( $O_{\text{coal}}$ ) on the coal surface with a truncation radius of 20 Å was calculated using RDF.

The peak and distance of the RDF of  $H_{\text{water}}$  around  $O_{\text{coal}}$  can reflect the effect of coal surface oxygen on the adsorption behavior of water molecules. The RDF of oxygen and water molecules on the coal surface in Fig. 8 reveals that the 1st strong peak appears near 1.85 Å when water molecules are adsorbed on the coal surface, which is caused by the strong hydrogen bonds formed between the oxygen-containing functional groups and water molecules on the coal surface. This effect enhances the adsorption of water molecules on the coal surface, thus

enhancing the surface wettability. The 2nd peak is near 3.25 Å due to the weak hydrogen bonding formed between oxygen-containing functional groups and water molecules. Yuan *et al.*<sup>11</sup> found that hydrogen bonding based on the distance between the donor and acceptor was less than 3.3 Å and the angle between donor-hydrogen-acceptor was greater than 120°. Under this criterion, the statistics of the number of hydrogen bonds were 62 (A), 91 (B) and 29 (C). Deducting the strong hydrogen bonds (A: 36; B: 50; C: 15), the number of weak hydrogen bonds in the three systems was found to be 26, 41 and 14, respectively, which are smaller than the number of strong hydrogen bonds and are consistent with the RDF peak height trends.

The hydrogen bonding between the phenolic hydroxyl group and water on the coal surface is shown schematically in Fig. 9. The hydrogen of the hydroxyl group can bond with three water molecules, with strong hydrogen bonding at 1.80 Å and 1.88 Å, and weak hydrogen bonding at 2.89 Å. It can be seen that the hydrogen bonding ability of the oxygen-containing functional groups on the coal surface with water molecules varies at different adsorption sites. In summary, the molecular dynamics simulation results further reveal the strong correlation of the wettability of the coal surface and the hydrogen bonding interaction between the oxygen-containing functional groups on the coal surface and water molecules. The hydrogen bonding enhances the coal–water interaction and the migration and diffusion of water molecules toward the coal surface, which finally enhances the coal surface wettability.

### Density functional theory calculation

The Dmol3 module in Materials Studio software was used to establish the adsorption models of different skeletal structures and water molecules on the coal surface, and the adsorption energy and adsorption distance of water molecules on the adsorption sites of aromatic and aliphatic hydrocarbon

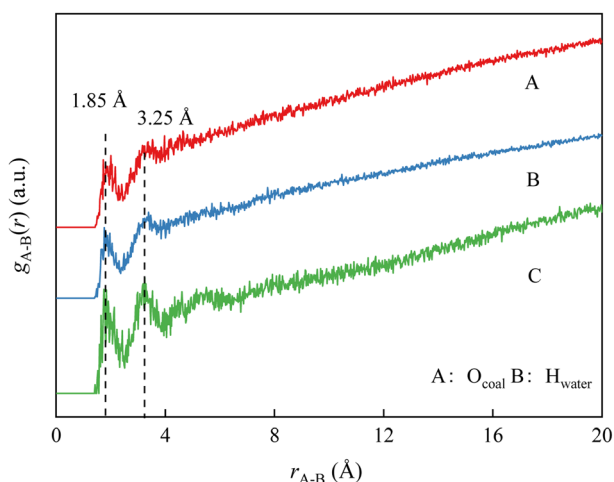


Fig. 8 RDF for oxygen atoms on the coal surface with the hydrogen atom of water.

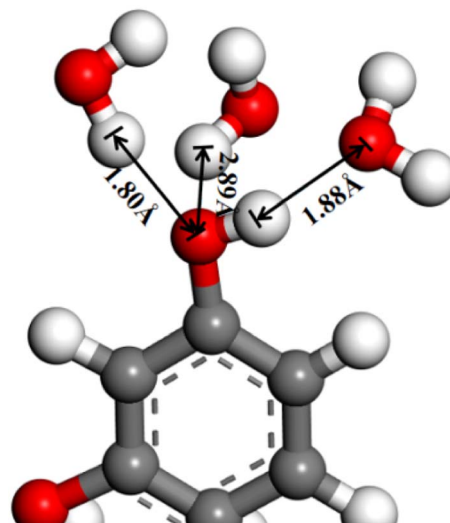


Fig. 9 Schematic diagram of the hydrogen bond between the phenol hydroxyl group on the coal surface and water.

structures were calculated based on the quantum chemical density functional theory to explore the microscopic mechanisms of organic molecular skeletal structure differences on the wettability of the coal surface.

The molecular models and interaction configurations are structurally optimized and the energies and interaction distances are analyzed. The Perdew–Burke–Ernzerhof (PBE) generalized gradient approximation (GGA)-based electron exchange-correlation generalized function is used without restricting the electron spin; the convergence criteria of energy, force, and displacement during the self-consistency are  $2.0 \times 10^{-5}$  hartree, 0.004 hartree per Å, and 0.005 Å, respectively. The adsorption energy between two molecules is defined as

$$\Delta E = E_{A+B} - E_A - E_B \quad (5)$$

where  $E_{A+B}$  is the total energy of two molecules after adsorption,  $\text{kJ mol}^{-1}$ ;  $E_A$  and  $E_B$  are the energies of molecule A and molecule B, respectively,  $\text{kJ mol}^{-1}$ . The negative value of  $\Delta E$  denotes the exothermic interaction process, with the larger absolute value indicative of the easier interaction.

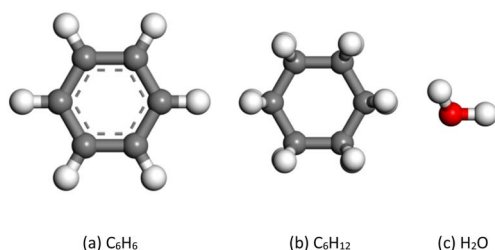


Fig. 10 Molecular models: (a) benzene, (b) cyclohexane and (c) water molecule.

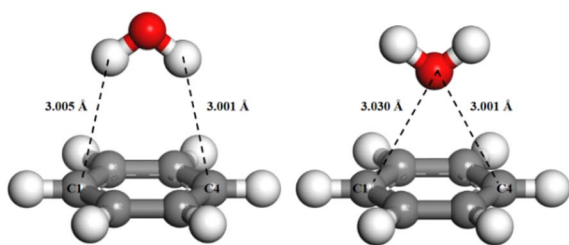


Fig. 11 Initial adsorption configuration of water molecules in bituminous coal.

The structurally optimized models used for DFT calculations are shown in Fig. 10. Benzene and cyclohexane are the most basic aromatic and aliphatic hydrocarbon structural units to represent the molecular molecule of bituminous coals without the interference of other groups at the same time.

When designing the adsorption models of different skeletal structures and water molecules on the coal surface, the adsorption configuration of water molecules was positioned above the plane with benzene and cyclohexane, where the water molecule is located in the center of the ring and the two hydrogen atoms are opposite the carbon atoms C1 and C4. Two adsorption configurations of water molecules on the coal surface were considered: the two hydrogen atoms of the water molecule facing upward and downward (Fig. 11).<sup>30</sup>

Molecular dynamics simulation *supra* has verified that the wettability difference across the three groups of bituminous coals was related to the hydrogen bonding interaction between coal and water, and that the strength of hydrogen bonding directly affected the wettability of the coal surface. To quantitatively analyze the interaction between aromatic and aliphatic hydrocarbon structures and water, the interaction conformations were constructed with optimized benzene, cyclohexane and water molecules to determine the adsorption energy, as shown in Table 7.

The adsorption energies of water molecules on different skeletal structures are negative, indicating that water molecules are spontaneously adsorbed at the aromatic and aliphatic hydrocarbon structures on the coal surface. Among various adsorption modes, the adsorption energy of water molecules with hydrogen atoms facing downward is the most negative,  $-24.43 \text{ kJ mol}^{-1}$ , which is much smaller than that of the adsorption conformation of water molecules with hydrogen atoms facing upward ( $-2.15 \text{ kJ mol}^{-1}$ ).

The adsorption energy of water molecules with aliphatic hydrocarbon structures with hydrogen atoms facing downward is  $-8.84 \text{ kJ mol}^{-1}$ , which is also smaller than that of the adsorption conformation of water molecules with hydrogen atoms facing upward ( $-4.62 \text{ kJ mol}^{-1}$ ), suggesting that the hydrogen atom-facing downward water molecule adsorption conformation on different skeletal structures is the most stable.

When water molecules are adsorbed in a more stable adsorption configuration, the adsorption energy of water molecules is much greater on the aromatic hydrocarbon structure than on the aliphatic hydrocarbon structure, indicating that the interaction of water molecules at the aromatic

Table 7 Adsorption energy of water molecules on different skeleton structures

Structure	Water molecular adsorption mode	Adsorption energy ( $\text{kJ mol}^{-1}$ )
Aromatic hydrocarbon structure	Hydrogen atoms facing up	-2.15
	Hydrogen atoms facing downward	-24.43
Aliphatic hydrocarbon structure	Hydrogen atoms facing up	-4.62
	Hydrogen atoms facing downward	-8.84



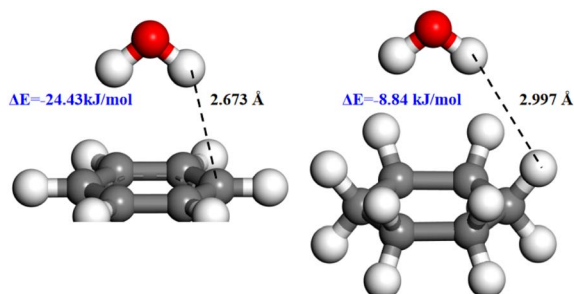


Fig. 12 Equilibrium configurations of interactions.

hydrocarbon structure on the coal surface was stronger. The interaction distances between two nearest atoms of water molecules and the aromatic and aliphatic hydrocarbon structures were measured, on the adsorption equilibrium configurations (Fig. 12).

The interaction distance between the aromatic hydrocarbon structure and water (2.673 Å) is smaller than that between the aliphatic hydrocarbon structure and water (2.997 Å), which indicates that water molecules are more easily adsorbed at the aromatic hydrocarbon structure on the coal surface, which is consistent with the previous conclusions of the carbon skeleton analysis and wettability analysis of the coal surface.

## Analysis of the free energy wetting mechanism based on the coal surface

Microscopically, the wetting is innately caused by the attractive forces between solid surface molecules and water molecules.<sup>31</sup> To investigate the mechanism of microscopic wetting action on the coal surface, surface free energy was analyzed for coal samples. Based on the measured contact angles, the van Oss–Chaudhury–Good theory was used to calculate the coal surface free energy.<sup>32–34</sup> The total surface free energy of the solids was decomposed into the nonpolar Lifshitz–van der Waals component and the polar Lewis acid–base component, and their relationship can be expressed as follows:

$$\gamma_s = \gamma_s^{\text{LW}} + \gamma_s^{\text{AB}} = \gamma_s^{\text{LW}} + 2\sqrt{\gamma_s^+ \gamma_s^-} \quad (6)$$

where  $\gamma_s$  is the total surface free energy,  $\text{mJ m}^{-2}$ ;  $\gamma_s^{\text{LW}}$  is the non-polar Lifshitz–van der Waals component, mainly dispersion, but also possible induction and orientation,  $\text{mJ m}^{-2}$ ;  $\gamma_s^{\text{AB}}$  is the polar Lewis acid–base component, mainly hydrogen bonding, which can be further divided into Lewis acidic and basic forces,  $\text{mJ m}^{-2}$ . Solid surface energy, liquid surface tension and the equilibrium contact angle are related by

$$\left( \gamma_1^{\text{LW}} + 2\sqrt{\gamma_1^+ \gamma_1^-} \right) (1 + \cos \theta) = 2 \left( \sqrt{\gamma_s^{\text{LW}} \gamma_1^{\text{LW}}} + \sqrt{\gamma_s^+ \gamma_1^-} + \sqrt{\gamma_s^- \gamma_1^+} \right) \quad (7)$$

where  $\theta$  is the measured equilibrium contact angle of the solid ( $^\circ$ );  $\gamma_1$  is the surface tension of the liquid,  $\text{mN m}^{-1}$ ;  $\gamma_1^{\text{LW}}$  is the

Lifshitz–van der Waals fraction of the liquid,  $\text{mN m}^{-1}$ ;  $\gamma_1^+$  is the Lewis acid fraction of the liquid,  $\text{mN m}^{-1}$ ;  $\gamma_1^-$  is the Lewis base fraction of the liquid,  $\text{mN m}^{-1}$ . The solid–liquid interface interaction free energy includes the Lifshitz–van der Waals interaction free energy as well as the Lewis acid–base interaction free energy, *i.e.*,<sup>33</sup>

$$\Delta G_{\text{sl}} = \Delta G_{\text{sl}}^{\text{LW}} + \Delta G_{\text{sl}}^{\text{AB}} = -2 \left( \sqrt{\gamma_s^{\text{LW}} \gamma_1^{\text{LW}}} + \sqrt{\gamma_s^+ \gamma_1^-} + \sqrt{\gamma_s^- \gamma_1^+} \right) \quad (8)$$

Diiodomethane contains only non-polar components and can be used as a standard liquid for determining the non-polar components of surface free energy. Formamide and deionized water contain both polar and non-polar components in their surface tensions and can be used as a standard liquid for determining the polar components of surface free energy, and their physical parameters are shown in Table 8.

The final free energy components are shown in Table 9. According to the classification criteria of van-Oss and Giese,  $\gamma_s^- < 28 \text{ mJ m}^{-2}$  is considered as a hydrophobic surface.<sup>35</sup> The  $\gamma_s^-$  of coal samples is much less than  $28 \text{ mJ m}^{-2}$ , which is consistent with the characteristics of a hydrophobic surface, indicating that all coal samples are hydrophobic bituminous coal. The  $\gamma_s^{\text{LW}}$  of coal samples is much higher than the  $\gamma_s^{\text{AB}}$ , which indicates that the surface of coal samples is mainly composed of non-polar Lifshitz–van der Waals components, which is

Table 8 Physical parameters of standard liquids at 20 °C

Standard liquid	Physical parameters ( $\text{mN m}^{-1}$ )			
	$\gamma_1$	$\gamma_1^{\text{LW}}$	$\gamma_1^+$	$\gamma_1^-$
Distilled water	72.8	21.8	25.5	25.5
Formamide	57.4	39	2.28	39
Diiodomethane	50.8	50.8	0	0

Table 9 Surface free energy composition of samples at 20 °C

Coal sample	Surface free energy ( $\text{mJ m}^{-2}$ )				
	$\gamma_s$	$\gamma_s^{\text{LW}}$	$\gamma_s^+$	$\gamma_s^-$	$\gamma_s^{\text{AB}}$
A	44.36	42.35	1.10	0.92	2.01
B	49.75	42.71	1.59	7.78	7.04
C	36.40	35.60	0.52	0.31	0.80

Table 10 Interfacial interactive free energy between coal samples and water

Coal sample	Free energy ( $\text{mJ m}^{-2}$ )		
	$\Delta G_{\text{sl}}^{\text{LW}}$	$\Delta G_{\text{sl}}^{\text{AB}}$	$\Delta G_{\text{sl}}$
A	−60.77	−20.27	−81.04
B	−61.03	−40.92	−101.95
C	−55.72	−12.89	−68.61



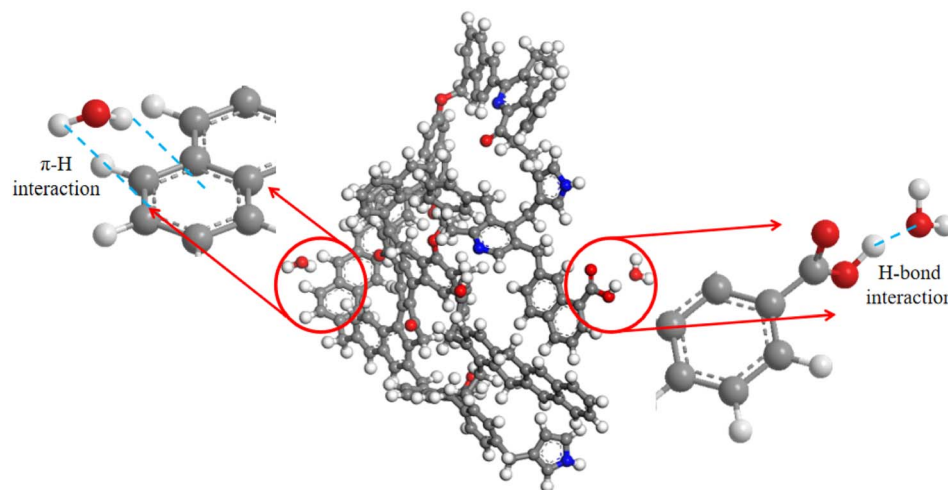


Fig. 13 Schematic diagram of coal–water system balance (C group).

consistent with our results of  $^{13}\text{C}$  NMR and XPS tests. Thus, the coal of the Pingdingshan coal mining area is a hydrophobic bituminous coal with the main non-polar aromatic hydrocarbon structure.

The  $\gamma_s$ ,  $\gamma_s^{\text{LW}}$  and  $\gamma_s^{\text{AB}}$  on the surface of the coal sample are  $B > A > C$  in descending order, which are positively correlated with wettability. The larger the free energy polar component on the surface of the coal sample, the greater the probability of hydrogen bonding with water molecules, and the better the wettability of the coal surface. The larger the non-polar component, the stronger the non-polar van der Waals interaction on the coal surface, which enhances the interaction between coal and water molecules, and thus the coal surface wettability.

To study the wetting mechanism of the coal surface, the interfacial interaction energy between the coal sample and water was further investigated by eqn (8), and the results are shown in Table 10.

As can be seen from Table 10, the Lifshitz–van der Waals interaction free energy and Lewis acid–base interaction free energy for all coal–water systems are less than zero, indicating that the van der Waals forces and polar interactions between coal samples and water have attractive effects, which originate from the combined effects of dispersion forces, orientation forces (electrostatic forces), induction forces and exchange forces between atoms and molecules. The hydrogen bonding as the polar component (Lewis acid–base interactions) is the main driving force leading to hydrophilicity on the coal surface.<sup>36</sup>

The absolute values of  $\Delta G_{\text{sl}}^{\text{LW}}$  and  $\Delta G_{\text{sl}}^{\text{AB}}$  of the three groups of coal samples decrease from B, to A and to C, and the van der Waals force and Lewis acid–base force are positively correlated with the wettability; that is, the greater the interaction force between coal and water, the better the surface wettability. The ability to form a hydrogen bond between coal and water is largest in group B and weakest in group C, suggesting the strongest and worst wettability, respectively.

Although the three groups of bituminous coals had poor wetting performance, the van der Waals forces and polar interactions between coal samples and water still have attractive

effects. All the above data validate that the surface free energy of coal can directly determine the strength of its attraction to water, while the elements and internal structure of coal samples have some influence on the surface free energy, which in turn affects the surface wettability of coal. Taking the molecular dynamics equilibrium configuration of the coal–water system of group C as an example, the  $\pi$ -H interaction and hydrogen bonding interaction are schematically shown in Fig. 13. The aromatic carbon content of the three bituminous coals is positively correlated with the van der Waals interactions in the surface free energy of coal, indicating the pivotal role of the aromatic hydrocarbon structure. This is because the aromatic hydrocarbon structure can produce strong water adsorption *via* stronger  $\pi$ -H bonding, which enhances the coal surface wettability. Hydrogen bonding is positively attributed to the main interaction between the surface oxygen-containing functional groups and water molecules.

## Conclusions

This paper presents the results of tests conducted on the molecular structure characteristics of bituminous coal and the effects of different carbon skeleton functional groups on bituminous coal wettability. Combining experimental methods with molecular simulations, we could conduct a more in-depth study of the wetting mechanism of coal dust, which is of great importance for the prevention of coal dust.

X-ray photoelectron spectroscopy (XPS) and nuclear magnetic resonance carbon spectroscopy ( $^{13}\text{C}$  NMR) clarified the bituminous coal construction: the surface aromatic hydrocarbon structure as the main skeleton, the oxygen-/nitrogen-containing functional groups and aliphatic hydrocarbons in the form of side chains linking aromatic hydrocarbon structural units, and the heteroatom oxygen and nitrogen in the form of phenolic hydroxyl and ether oxygens, pyrrole and pyridine.

The results of contact angle measurements and proximate analyses revealed that the fixed carbon content is the main factor affecting the wettability of bituminous coal. Combined





with the XPS experiment and NMR experiment, the more oxygen and aromatic carbon in all bituminous coal scans evoke the better wettability, and a contrary trend occurs for the fixed carbon aliphatic carbon content. Molecular dynamics simulations disclose that the altered wetting mainly stems from the hydrogen bonding of surface hydrophilic functionalities with water molecules. The density functional theory calculations found that the aromatic hydrocarbon structures can more effectively augment the water adsorption and consequent wetting performance than the aliphatic hydrocarbon structure.

For the free energy composition analysis, the experimental result verifies that hydrogen bonding positively relates to the leading interaction between surface oxo-moieties and water molecules. The aromatic carbon content is positively correlated with the van der Waals interaction between coal and water and thus the wettability. The hydrogen bonding enhances the Lewis acid–base interactions between coal and water, causing the migration and diffusion of water molecules toward the coal surface, which enhances the coal surface wettability. In addition, the aromatic hydrocarbon structure can enhance the van der Waals interactions *via*  $\pi$ -H bonding, which also contributes to the wettability of coal dust.

## Conflicts of interest

There are no conflicts to declare.

## Acknowledgements

This work was supported by the National Natural Science Foundation of China (52274172).

## References

- 1 Y. Li, X. Yang, Q. Ran, H. Wu, M. Irfan and M. Ahmad, *Environ. Sci. Pollut. Res. Int.*, 2021, **28**, 64606–64629.
- 2 P. Cai, W. Nie, D. Chen, S. Yang and Z. Liu, *Fuel*, 2019, **239**, 623–635.
- 3 P. D. Blanc and A. Seaton, *Am. J. Respir. Crit. Care Med.*, 2016, **193**, 603–605.
- 4 Y. Ji, T. Ren, P. Wynne, Z. Wan, Z. Ma and Z. Wang, *Int. J. Min. Sci. Technol.*, 2016, **26**, 199–208.
- 5 C. Xu, D. Wang, H. Wang, H. Xin, L. Ma, X. Zhu, Y. Zhang and Q. Wang, *Powder Technol.*, 2017, **318**, 33–39.
- 6 W. Cheng, G. Zhou, L. Chen, G. Wang, W. Nie and Q. Zhang, *Coal Sci. Technol.*, 2020, **48**, 1–20, in Chinese.
- 7 Z. Luo, M. Fan, Y. Zhao, X. Tao, Q. Chen and Z. Chen, *Powder Technol.*, 2008, **187**, 119–123.
- 8 W. Cheng, J. Xue, G. Zhou, W. Nie and J. Wen, *J. China Univ. Min. Technol.*, 2016, **45**, 462–468, in Chinese.
- 9 H. Wang, L. Zhang, D. Wang and X. He, *Adv. Powder Technol.*, 2017, **28**, 3130–3139.
- 10 X. Jingna, N. Guanhua, X. Hongchao, L. Shang, S. Qian and D. Kai, *Powder Technol.*, 2019, **356**, 263–272.
- 11 M. Yuan, W. Nie, H. Yu, J. Yan, Q. Bao, W. Zhou, Y. Hua, L. Guo and W. Niu, *J. Environ. Chem. Eng.*, 2021, **9**, 105986.
- 12 B. Li, S. Liu, M. Fan and L. Zhang, *Powder Technol.*, 2019, **344**, 684–692.
- 13 J. Meng, L. Wang, S. Zhang, Y. Lyu and J. Xia, *Chem. Phys. Lett.*, 2021, **785**, 139130.
- 14 W. Feng, Z. Li, H. Gao, Q. Wang, H. Bai and P. Li, *Green Energy Environ.*, 2021, **6**, 150–159.
- 15 Y. Zhang, S. Hu, Q. Zhong, J. Zhuo and J. P. Mathews, *Fuel*, 2021, **295**, 120616.
- 16 Y. Liu, H. Li, M. Gao, S. Ye, Y. Zhao, J. Xie, G. Liu, J. Liu, L. Li, J. Deng and W. Zhou, *RSC Adv.*, 2021, **11**, 24543–24555.
- 17 C. Semprebbon, G. McHale and H. Kusumaatmaja, *Soft Matter*, 2016, **13**, 101–110.
- 18 Z. Zhao, C. Yang, C. Sun and X. Shu, *J. China Coal Soc.*, 2011, **36**, 442–446, in Chinese.
- 19 X. Wang, S. Yuan and B. Jiang, *Adv. Powder Technol.*, 2019, **30**, 1696–1708.
- 20 J. Zhang, H. Li, Y. Liu, X. Li, J. Xie, S. Ye, L. Luming, W. Zhou, Y. Zhao and H. Hao, *J. China Coal Soc.*, 2021, **46**, 812–825, in Chinese.
- 21 D. V. Franco, J. M. Gelan, H. J. Martens and D. J.-M. Vanderzande, *Fuel*, 1991, **70**, 811–817.
- 22 M. J. Trehwella, I. J. F. Poplett and A. Grint, *Fuel*, 1986, **65**, 541–546.
- 23 D. Guo, J. Ye, Q. Wang and X. Guo, *J. China Coal Soc.*, 2016, **41**, 3040–3046, in Chinese.
- 24 X. Cao, M. A. Chappell, A. Schimmelmann, M. Mastalerz, Y. Li, W. Hu and J. Mao, *Int. J. Coal Geol.*, 2013, **108**, 53–64.
- 25 Q. Yao, C. Xu, Y. Zhang, G. Zhou, S. Zhang and D. Wang, *Process Saf. Environ. Prot.*, 2017, **111**, 726–732.
- 26 A. Kozbial, F. Zhou, Z. Li, H. Liu and L. Li, *Acc. Chem. Res.*, 2016, **49**, 2765–2773.
- 27 R. Zhang, Y. Xing, Y. Xia, J. Luo, J. Tan, G. Rong and X. Gui, *Appl. Surf. Sci.*, 2020, **511**, 145610.
- 28 W. Xia, J. Yang and C. Liang, *Appl. Surf. Sci.*, 2014, **293**, 293–298.
- 29 R. Liu, G. Zhou, C. Wang, W. Jiang and X. Wei, *J. Hazard. Mater.*, 2020, **397**, 122734.
- 30 S. Li, V. R. Cooper, T. Thonhauser, A. Puzder and D. C. Langreth, *J. Phys. Chem. A*, 2008, **112**, 9031–9036.
- 31 A. Steele, I. Bayer and E. Loth, *Nano Lett.*, 2009, **9**, 501–505.
- 32 C. J. V. Oss, R. J. Good and R. J. Busscher, *J. Dispersion Sci. Technol.*, 1990, **11**, 75–81.
- 33 C. J. Van Oss, R. J. Good and M. K. Chaudhury, *Langmuir*, 1988, **4**, 884–891.
- 34 C. J. van Oss and R. F. Giese, *J. Dispersion Sci. Technol.*, 2005, **25**, 631–655.
- 35 C. J. V. Oss and R. F. Giese, *Clays Clay Miner.*, 1995, **43**, 474–477.
- 36 X. Gui, Y. Xing, T. Wang, Y. Cao, Z. Miao and M. Xu, *Powder Technol.*, 2017, **305**, 109–116.

